Available online at www.sciencedirect.com
ScienceDirect
Journal of Sound and Vibration 323 (2009) 214–231
JOURNAL OF SOUND AND VIBRATION
www.elsevier.com/locate/jsvi

The dynamics of variants of two-dimensional cantilevered flexible plates in axial flow

Liaosha Tang[a,c,*], Michael P. Païdoussis[b], Jin Jiang[c]

[a]*Institute for Aerospace Studies, University of Toronto, 4925 Dufferin St., Toronto, Ontario, Canada M3H 5T6*
[b]*Department of Mechanical Engineering, McGill University, 817 Sherbrooke St. W., Montréal, Québec, Canada H3A 2K6*
[c]*Hubei Key Laboratory of Fluid Machinery and Power Equipment Technology, Wuhan University, 8 Donghu St. S., Wuahn, Hubei 430072, PR China*

Received 4 April 2008; received in revised form 12 December 2008; accepted 17 December 2008
Handling Editor: S. Bolton
Available online 5 February 2009

Abstract

Cantilevered thin flexible plates in subsonic axial flow may lose dynamic stability at sufficiently high flow velocity. Once the critical point is exceeded, flutter takes place, and the flutter amplitude grows as the flow velocity is further increased. Richer dynamics are obtained for modified forms (''variants'') of this basic system. In particular, in the present paper four cases are considered: with (i) gravity, (ii) a spring support of either linear or cubic type, (iii) a concentrated mass mounted on the plate, and (iv) a small oscillating incidence angle in the undisturbed flow. For each specific variant of the basic system, the influence of these added features is investigated; e.g., for the spring support and concentrated mass the effects of magnitude and/or location are discussed. Some interesting phenomena found in the dynamics of these variants of the system are summarized in this paper.

1. Introduction

The dynamics of thin cantilevered flexible plates in axial flow is one the classical problems of Applied Mechanics [1]. Some of the early work was concerned with the flapping of flags [2,3] and the dynamics of aircraft and missile skins, particularly in supersonic flow [4]. More recently, there has been renewed interest in the dynamics of cantilevered, typically long, plates in incompressible flow, not only as an abstract problem, but also for engineering applications, e.g., in paper-making [5–7], for electricity generation [8], for aircraft control [9] and in biomimesis [10].

The present paper summarizes some recent research conducted by the authors on the dynamics of two-dimensional thin cantilevered plates in subsonic axial flow. The two-dimensional plate is modelled as a beam with an inextensible centreline, and an unsteady lumped vortex model is used to calculate the pressure difference across the oscillating plate. The analysis of system dynamics is carried out in the time-domain.

*Corresponding author at: Institute for Aerospace Studies, University of Toronto, 4925 Dufferin St., Toronto, Ontario, Canada M3H 5T6. Tel.: +1 416 6677701; fax: +1 416 6677799.
E-mail address: ltang2008@gmail.com (L. Tang).

0022-460X/$ - see front matter © 2008 Elsevier Ltd. All rights reserved.
doi:10.1016/j.jsv.2008.12.020

The system loses stability by flutter at sufficiently high flow velocity, and both the instability threshold, as a function of the system parameters, and the post-critical behaviour of the system have recently been studied extensively by Tang and Païdoussis [11].

Four variants of the system are studied in the present paper: in the presence of (i) gravity, (ii) a spring support, linear or nonlinear, somewhere along the plate, (iii) a concentrated mass at various locations along the length of the plate, and (iv) a small oscillating angle of incidence of the undisturbed flow. This research is not only curiosity-driven; it is also related to the design of a new type energy-harvesting device, which is presented in another paper by the same authors [12]. It will be shown in the present paper that the dynamics of the system, taking into account gravity, a spring support, a concentrated mass or an oscillating incidence angle, is qualitatively altered; moreover, some interesting phenomena can be observed, not present in the basic system (in the absence of these features).

2. The basic system

A schematic diagram of a cantilevered flexible plate in axial flow is shown in Fig. 1. The geometrical characteristics of the rectangular homogeneous plate are the length of the flexible section L, width B and thickness h; $B \to \infty$ and $h \ll L$ for a two-dimensional thin plate. Normally, there is a rigid segment of length L_0 as part of the clamping arrangement at the upstream end. The other physical parameters of the system are the plate material density ρ_P and bending stiffness $D = Eh^3/\sqrt{12(1-\nu^2)}$ (where E and ν are, respectively, Young's modulus and the Poisson ratio of the plate material), the fluid density ρ_F, and the undisturbed flow velocity U. As shown in Fig. 1, W and V are, respectively, the transverse and longitudinal (axial) displacements of the plate. F_L and F_D are the aero/hydro-dynamic loads acting on the plate in the transverse and longitudinal directions, respectively; S is the distance of a material point on the plate from the origin, measured along the plate centreline in a coordinate system embedded in the plate. Moreover, material damping of the Kelvin–Voigt type is considered with the loss factor denoted by a.

The equations of motion of the plate can be written in nondimensional form as [11]

$$\ddot{w} + \left(1 + \alpha\frac{\partial}{\partial\tau}\right)[w''''(1+w'^2) + 4w'w''w''' + w''^3] + w'\int_0^s (\dot{w}'^2 + w'\ddot{w}')\,\mathrm{d}s - w''\int_s^1\left[\int_0^s (\dot{w}'^2 + w'\ddot{w}')\,\mathrm{d}s\right]\mathrm{d}s = f_{\mathrm{eff}}, \tag{1}$$

$$v = -\frac{1}{2}\int_0^s w'^2\,\mathrm{d}s, \tag{2}$$

$$f_{\mathrm{eff}} = \mu U_R^2\left(f_L - w'f_D + w''\int_s^1 f_D\,\mathrm{d}s\right), \tag{3}$$

where the overdot and the prime represent $\partial(\,)/\partial\tau$ and $\partial(\,)/\partial s$, respectively. The nondimensional variables are defined by

$$x = \frac{X}{L}, \quad y = \frac{Y}{L}, \quad w = \frac{W}{L}, \quad v = \frac{V}{L}, \quad s = \frac{S}{L}, \quad l_0 = \frac{L_0}{L},$$

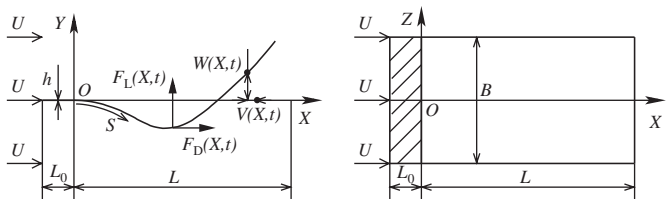

Fig. 1. A cantilevered flexible plate in axial flow.

$$\tau = \frac{t}{\sqrt{\rho_P h L^4/D}}, \quad \alpha = \frac{a}{\sqrt{\rho_P h L^4/D}}, \quad f^\star = f\sqrt{\rho_P h L^4/D},$$

$$f_L = \frac{F_L}{\rho_F U^2}, \quad f_D = \frac{F_D}{\rho_F U^2}, \tag{4}$$

where $f^\star$ and f are, respectively, nondimensional and dimensional vibration frequencies. Moreover, the mass ratio μ and the reduced flow velocity U_R are defined by

$$\mu = \frac{\rho_F L}{\rho_P h}, \quad U_R = UL\sqrt{\frac{\rho_P h}{D}}. \tag{5}$$

In Eq. (3), the aero/hydro-dynamic loads are calculated using the unsteady lumped vortex model [11]. On each individual panel, the nondimensional pressure difference across the plate Δp is first computed and then decomposed into the *lift* f_L and the *drag* f_D. That is

$$f_{Li} = \Delta p_i \cos\alpha_i, \quad f_{Di} = \Delta p_i \sin\alpha_i + C_D, \tag{6}$$

where α_i is the angle of incidence of the ith panel. An additional drag coefficient C_D, uniformly distributed over the length of the plate, may be considered in f_D to account for the *viscous* effects of the fluid flow (refer to Ref. [11] for details).

The analytical model of the basic system has first been validated against available experimental data for the flutter threshold. It has been shown that the level of agreement is superior to that achieved by other theories [11], though still not sufficiently good—with theory generally under-predicting the flutter threshold. This discrepancy between theoretical predictions and experimental observations has been attributed to the lack of a proper accounting of (viscous) aero/hydro-dynamic drag in the theory, which would increase the tension in the plate and thus the stability threshold of the system. Another prominent "weakness" of all theories, including ours, is that they fail to predict the subcritical nature of the bifurcation and the strong hysteresis observed in the experiments [13,14]. One possible explanation may be that all experiments are conducted in a wind or water tunnel, while theories (e.g., Refs. [11,14]) normally consider open flow. However, the reason causing the observed subcritical bifurcation may be more complex (see Ref. [11] for details); the exact underlying mechanism is still an open question.

As already shown in Ref. [11] for a specific system with $\mu = 0.2$, the dynamics of the *basic* system, without gravity or an oscillating incidence angle and without additional springs or masses, is relatively simple. When U_R is below the critical point U_{Rc}, the plate remains straight; any small disturbance to the system is attenuated. Once U_R exceeds U_{Rc}, flutter occurs, and the flutter amplitude grows as U_R increases further.

3. With gravity

No gravity is considered for the basic system (see Eqs. (1) and (3)) because the plate is set up in the so-called "vertical configuration" [11]; the gravitational force is in the negative Z-direction of Fig. 1. However, when a plate is in the "horizontal configuration" [11] with the gravitational force pointing to the negative Y-direction, as in the design of a flexible control surface [9], it *has* to be taken into account. It follows that the effective force f_{eff} acting on the plate, i.e., Eq. (3) should be rewritten as

$$f_{\text{eff}} = \mu U_R^2 \left(f_L - w' f_D + w'' \int_s^1 f_D \, \mathrm{d}s \right) - \gamma_G. \tag{7}$$

In Eq. (7), γ_G is the gravity parameter, accounting for the ratio of the gravitational force to the restoring force of the plate, defined by

$$\gamma_G = \frac{(\rho_P - \rho_F) h g L^3}{D}, \tag{8}$$

where g is the gravitational acceleration.

To determine the value of the gravity parameter, the experiments conducted by Tang et al. [14] for a (basic) system set up in the vertical configuration are considered; supposing that only the plate length L varies, one obtains the corresponding values of μ and γ_G as listed in Table 1. It should be noted that, when the parameters $\rho_P = 2.84 \times 10^3\,\mathrm{kg/m^3}$ (aluminium-7075), $\rho_F = 1.226\,\mathrm{kg/m^3}$ (air), $h = 3.9 \times 10^{-4}\,\mathrm{m}$ and $D = 0.383\,\mathrm{N\,m}$ of the system are fixed, the mass ratio μ is proportional to L; while, the gravity parameter γ_G is proportional to L^3.

The influence of the gravitational force on the stability of the system is first examined using the parameters of Table 1. It can be seen in Table 2 that the system generally has a higher critical point U_{Rc} (note that flutter

Table 1
The mass ratio μ and gravity parameter γ_G of the system.

L (m)	$\mu = [\rho_F/(\rho_P h)]L$	$\gamma_G = [(\rho_P - \rho_F)gh/D]L^3$
0.181	0.2	0.167
0.452	0.5	2.61
1.81	2	167

Table 2
The influence of the gravitational force on system stability.

μ	γ_G	U_{Rc}	$U_{R_c^\star}$	$(U_{Rc} - U_{R_c^\star})/U_{R_c^\star}$ (%)
0.2	0.167	9.92	9.92	0
0.5	2.61	6.95	6.91	0.58
2	167	11.88	10.89	9.09

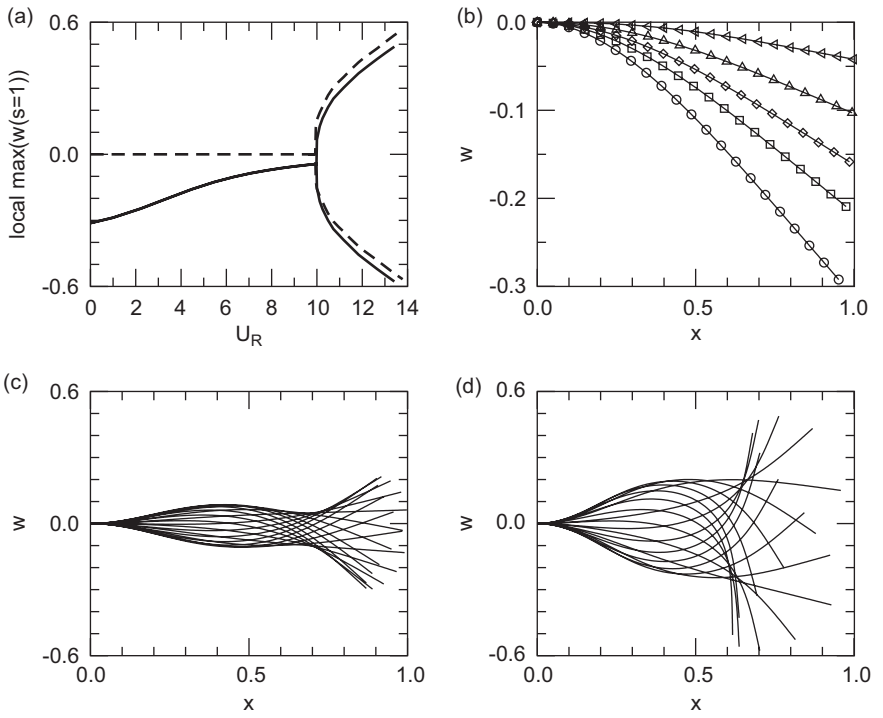

Fig. 2. The dynamics of horizontal system subject to gravity: (a) bifurcation diagram, (b) buckled states when $U_R < U_{Rc}$, (c) modes of small amplitude flutter at $U_R = 10.48$, and (d) modes of large amplitude flutter at $U_R = 13.42$. The other parameters are $\mu = 0.2$, $l_0 = 0.01$, $\alpha = 0.004$, $C_D = 0$ and $\gamma_G = 2.5$. In subfigure (a): solid line, $\gamma_G = 2.5$; dashed-line, $\gamma_G = 0$ (i.e., the basic system). In subfigure (b), the lines with various symbols: circle, $U_R = 0.02$; square, $U_R = 3.16$; diamond, $U_R = 4.47$; up-triangle, $U_R = 6.32$; left-triangle, $U_R = 9.95$.

takes place when $U_R > U_{Rc}$) than its counterpart $U_{R_c^\star}$ for the basic configuration, in which gravity is inoperative. Moreover, when the value of μ is small (i.e., the plate is short), γ_G is also small and so is the influence of the gravitational force. However, as γ_G increases sharply with increasing L, the gravitational force has a significant effect on the system dynamics for systems with a relatively large value of μ (i.e., the plate is relatively long). For example, when $\mu = 2$, $U_{Rc} = 11.88$ and $U_{R_c^\star} = 10.89$; the increase is as large as 9.09%.

Some aspects of the dynamics for $\mu = 0.2$ are illustrated in Fig. 2, where the gravity parameter is arbitrarily chosen as $\gamma_G = 2.5$ (considerably larger than $\gamma_G = 0.167$ in Table 2). It can be seen in Figs. 2(a) and (b) that the plate is buckled, by the effect of gravity alone, when $U_R = 0$; it remains buckled for all values of U_R until the onset of flutter. Note that, when U_R is close to zero, say $U_R = 0.02$ as shown in Fig. 2(b), the cantilevered flexible plate is statically deflected without flow. It is found that the shape of the buckled plate is always in the first beam mode for this case. With increasing U_R, the amplitude of the static deflection decreases; that is, the plate is elevated by the aero/hydro-dynamic loads and becomes flatter. Obviously, the buckled form of the plate is defined by the balance between four distributed forces: the gravitational force, the restoring force and the aero/hydro-dynamic *lift* f_L and *drag* f_D achieved for the buckled shape of the plate. Note that the drag force f_D results in the tension in the plate (see Eqs. (3) and (4) in Ref. [11]). As U_R is increased further, flutter takes place; the critical reduced flow velocity is $U_{Rc} = 9.98$, as seen in Fig. 2(a), which is a little higher than $U_{R_c^\star} = 9.92$ for the basic configuration. Moreover, it is interesting to find that flutter occurs directly from the buckled state; a stable flat state does not occur. Finally, when U_R exceeds the critical point, the flutter

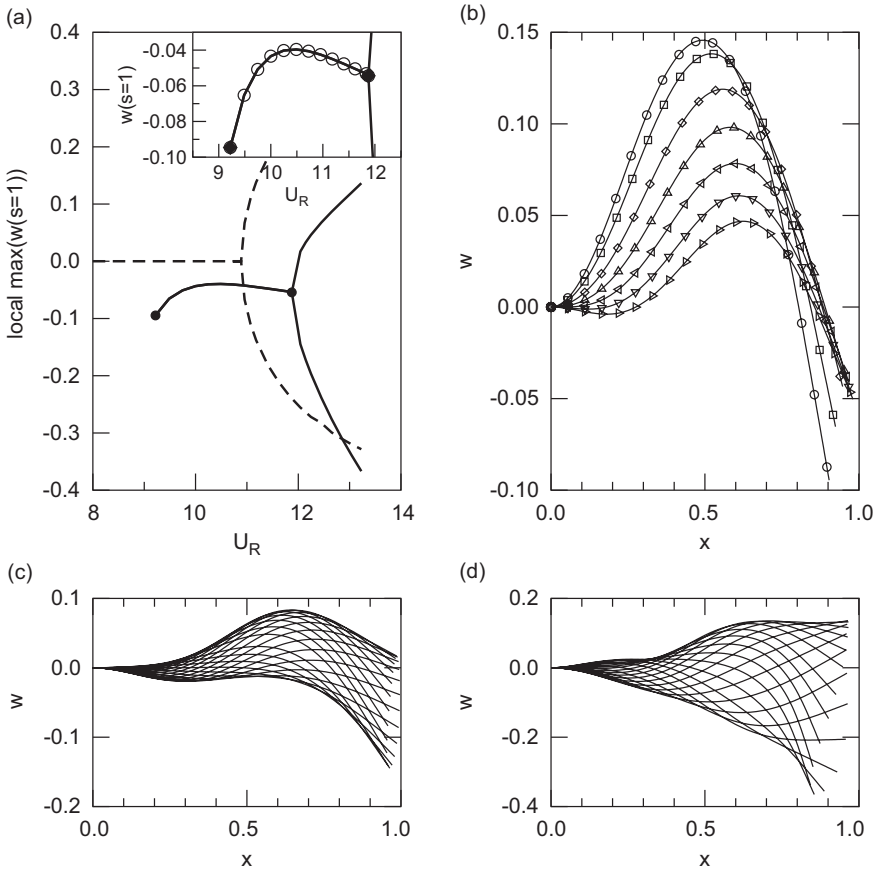

Fig. 3. The dynamics of horizontal system subject to gravity: (a) bifurcation diagram, (b) buckled states when $U_R < U_{Rc}$, (c) modes of small amplitude flutter at $U_R = 12.04$, and (d) modes of large amplitude flutter at $U_R = 13.2$. The other parameters are $\mu = 2$, $l_0 = 0.01$, $\alpha = 0.004$, $C_D = 0$ and $\gamma_G = 167$. In subfigure (a): solid line, $\gamma_G = 167$; dashed-line, $\gamma_G = 0$ (i.e., the basic system). In subfigure (b), the lines with various symbols: circle, $U_R = 9.92$; square, $U_R = 9.49$; diamond, $U_R = 10.0$; up-triangle, $U_R = 10.5$; left-triangle, $U_R = 11.0$; down-triangle, $U_R = 11.4$; right-triangle, $U_R = 11.8$.

amplitude increases with increasing U_R. Due to the influence of the gravitational force, the vibration modes of the system are not symmetric with respect to the mean flow axis (i.e., the x-axis).

As one can see in Table 1, the value of the gravity parameter γ_G increases very quickly as μ increases. The dynamics of the system with $\mu = 2$ and $\gamma_G = 167$ are shown in Fig. 3. From the bifurcation diagram of Fig. 3(a), the critical point in this case is $U_{Rc} = 11.88$, which is considerably larger than $U_{R_c^\star} = 10.89$ for $\gamma_G = 0$. When $U_R > U_{Rc}$, flutter takes place. As shown in Figs. 3(a), (c) and (d), the flutter amplitude increases with increasing U_R, and the vibration modes of the system are strongly asymmetric. The buckled states of the plate for $U_R < U_{R_c^\star}$ are shown in Fig. 3(b). It is very interesting to see that, when U_R approaches $U_{R_c^\star}$ from below, the plate is buckled in the second beam mode, in contrast to situation shown in Fig. 2(b) where the plate is buckled with a predominantly first-beam-mode shape. Moreover, in this case also, the static deflection of the plate is diminished with increasing U_R. But as the amplitude of buckling decreases, its shape becomes more complex, with the appearance of a third-beam-mode component. Accordingly, in the bifurcation diagram of amplitude of the plate tip versus U_R in Fig. 3(a), the curve first goes up and then somewhat drops with increasing U_R before the onset of flutter. It should be mentioned that, unlike the case shown in Fig. 2 for $\mu = 0.2$ and $\gamma_G = 2.5$ where the static deflection of the plate as $U_R \to 0$ can be obtained, for the case $\mu = 2$ and $\gamma_G = 167$ shown in Fig. 3, the present theory fails when $U_R < 8.94$: when the flow velocity is too low to lift the plate, the gravity-induced deflection is too large for the present structural model (Eqs. (1) and (2)) to yield a solution.

4. With a spring support

A schematic diagram of a cantilevered flexible plate with an additional (linear or cubic) spring support in axial flow is shown in Fig. 4, where S_S is the location of the spring, $F_S = -K_L W(S_S) - K_C W(S_S)^3$ is the spring force acting on the plate, and K_L and K_C are the stiffnesses of the linear or cubic spring, as the case may be. When the vibration amplitude is large, the longitudinal displacement of the plate, V, becomes important. In the present paper, the additional spring support is assumed to be free to move longitudinally with the plate; only transverse spring forces are considered. Therefore, the equations of motion of the plate are still given by Eqs. (1) and (2). However, instead of Eq. (3), the effective force f_{eff} acting on the plate should be calculated by

$$f_{\text{eff}} = \mu U_R^2 \left(f_L - w' f_D + w'' \int_s^1 f_D \, \mathrm{d}s \right) + f_S \delta(s - s_S), \tag{9}$$

where δ denotes the Dirac delta function, and $s_S = S_S/L$ is the location of the additional spring support normalized by the length of the flexible plate L. The nondimensional spring force f_S is given by

$$f_S = \frac{L^3}{D} F_S = -k_L w(s_S) - k_C w(s_S)^3, \tag{10}$$

where k_L and k_C are, respectively, the nondimensional stiffnesses of the linear and the cubic spring, defined by

$$k_L = \frac{L^4}{D} K_L, \quad k_C = \frac{L^6}{D} K_C; \tag{11}$$

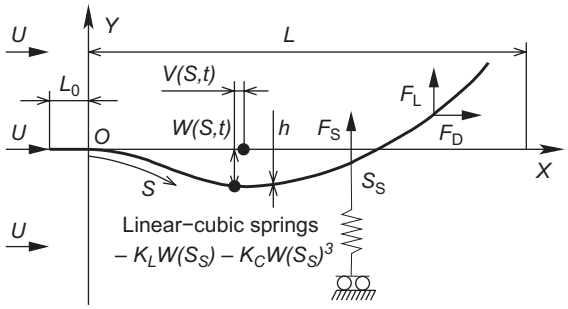

Fig. 4. A cantilevered flexible plate with an additional spring support in axial flow.

which represent the ratios of the spring forces to the flexural restoring force of the plate. It is stressed that in the calculations the spring is *either* linear or cubic, *so* that either k_C or k_L is zero in Eq. (10).

When a linear spring support is added, the plate may lose stability statically (by buckling or divergence instability) rather than by flutter. Stability diagrams of the system with an additional linear spring support at $s_S = 1$ and 0.8 are shown in Figs. 5 and 6, respectively. It is obvious that the system dynamics is dependent not only on the stiffness but also on the location of the spring.

When the linear spring support is located at $s_S = 1$, it can be seen in Fig. 5 that the plate loses stability through flutter at various values of U_R, provided $k_L < 59$; loss of stability through divergence (buckling) occurs when $k_L > 59$. For $k_L < 59$, the value of U_{Rc} increases with increasing k_L. On the other hand, when $k_L > 59$, U_{Rc} decreases as k_L increases; however, with further increase in k_L, a plateau is reached at $U_{Rc} = 11.30$, as shown in the inset of Fig. 5. This implies that a clamped/simply supported plate in axial flow will lose stability through buckling at $U_{Rc} = 11.30$ for the particular values of μ, l_0, α and C_D used in the calculations (see the caption of Fig. 5), since the linear spring support is equivalent to a simple support when

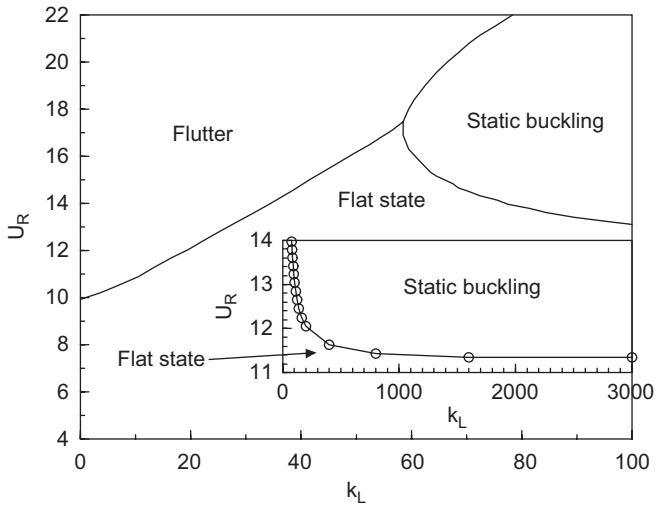

Fig. 5. Stability diagram of a cantilevered flexible plate in axial flow with an additional linear spring support at the plate trailing edge, i.e., $s_S = 1$. The system parameters are $\mu = 0.2$, $l_0 = 0.01$, $\alpha = 0.004$ and $C_D = 0$. The spring force is given by $f_S = -k_L w(s = 1)$.

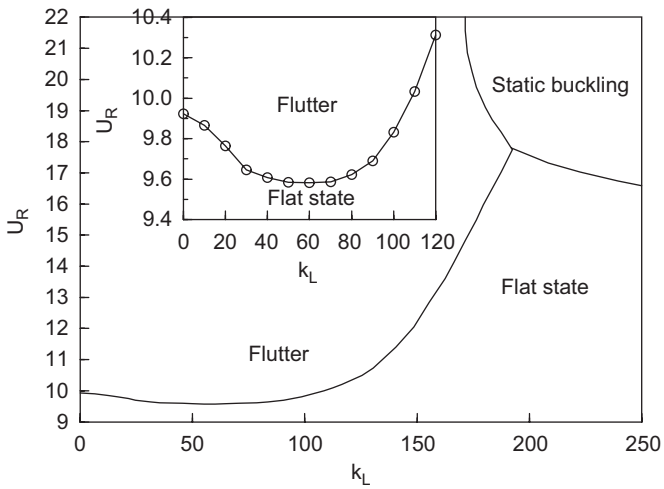

Fig. 6. Stability diagram of a cantilevered flexible plate in axial flow with an additional linear spring support at $s_S = 0.8$. The system parameters are $\mu = 0.2$, $l_0 = 0.01$, $\alpha = 0.004$ and $C_D = 0$. The spring force is given by $f_S = -k_L w(s = 0.8)$.

$k_L \to \infty$. Moreover, when $k_L > 59$, the plate may develop flutter at higher values of U_R, beyond the onset of buckling. It can be shown that all the limit cycle oscillations observed in the flutter region of Fig. 5 are of the symmetric type. At a given value of k_L, the flutter amplitude grows with increasing U_R. The plate cannot develop divergence (buckling) thereafter, beyond the flutter threshold in this range of k_L.

As seen in Fig. 6, the three stable states (i.e., stable flat state, static buckling and flutter) can also arise when $s_S = 0.8$. The plate loses stability through flutter when $k_L < 193$. For a range of k_L around $k_L = 193$, divergence may succeed flutter at higher U_R. But, when $k_L > 193$, the primary instability is buckling; flutter never takes place, no matter how large U_R is. Again, only symmetric limit cycle oscillations are found in the flutter region; at a fixed value of k_L, the flutter amplitude grows as U_R increases. A very interesting stronger-constraint/less-stable-system phenomenon can be observed in Fig. 6: the system loses stability at a lower critical point U_{Rc} when $0 < k_L < 106$ than when $k_L = 0$. In fact, when $0 < k_L < 56$, the value of U_{Rc} *decreases* as k_L *increases*.

If the additional spring support is cubic, it can be seen in Fig. 7 for the case $s_S = 0.8$ and $k_C = 6000$ that the system exhibits richer dynamics. The system still loses stability through flutter, but in a very abrupt manner, at $U_{Rc} = 9.92$. After the primary bifurcation, the system develops symmetric limit cycle oscillations, before a secondary bifurcation takes place at $U_R = 15.33$; beyond this point, the limit cycle oscillations become asymmetric. In the region of period-1 asymmetric limit cycle oscillation (i.e., $15.33 < U_R < 17.86$), it is interesting to see that the flutter amplitude of the plate trailing edge decreases with increasing U_R. A series of period-doubling bifurcations take place at $U_R = 17.86$, 18.49 and 18.74, followed by chaotic motions for $18.81 < U_R < 19.62$. However, as U_R is increased further, regular limit cycle oscillations re-emerge; another period-doubling route to chaos can be observed in the region $19.62 < U_R < 21.10$. The main region of chaos is for $21.10 < U_R < 23.45$; there is a periodic window between $U_R = 22.36$ and 22.56. Finally, the plate becomes statically buckled when $U_R > 23.45$.

5. With a concentrated mass

When there is an additional concentrated mass m_A at S_M on the plate, as illustrated in Fig. 8, the equation of motion of the plate, i.e., Eq. (1), should be rewritten as

$$\begin{aligned}&[1+\sigma_M\delta(s-s_M)]\ddot{w}+\left(1+\alpha\frac{\partial}{\partial\tau}\right)[w''''(1+w'^2)+4w'w''w'''+w''^3]\\&+[1+\sigma_M\delta(s-s_M)]w'\int_0^s(\dot{w}'^2+w'\ddot{w}')\,\mathrm{d}s\\&-w''\int_s^1[1+\sigma_M\delta(s-s_M)]\left[\int_0^s(\dot{w}'^2+w'\ddot{w}')\,\mathrm{d}s\right]\mathrm{d}s=f_{\mathrm{eff}},\end{aligned}\tag{12}$$

where the mass parameter σ_M is defined by

$$\sigma_M=\frac{m_A}{\rho_P hL};\tag{13}$$

it is the ratio of the concentrated mass to the mass of the plate itself (in the sense of the per-unit-width mass). Moreover, s_M is the location of the concentrated mass, normalized by the length of the flexible plate L, i.e., $s_M = S_M/L$.

The influence of an additional concentrated mass for various values of σ_M and s_M on stability is shown in Fig. 9. It can be seen in Fig. 9(a) that a small concentrated mass $\sigma_M = 0.01$ at a variety of locations along the length of the plate has different effects on the critical point. When there is no additional mass, i.e., for $s_M = 0$ (equivalent to the basic configuration), $U_{Rc} = 9.92$. When $s_M < 0.4$, the value of U_{Rc} decreases slightly with increasing s_M. When $0.4 < s_M < 0.7$, U_{Rc} grows with increasing values of s_M and reaches the maximum $U_{Rc} = 9.97$ at $s_M = 0.7$. Beyond this maximum point, U_{Rc} decreases again, more precipitously this time, as s_M increases further; finally, a minimum $U_{Rc} = 9.70$ is reached when the concentrated mass is at $s_M = 1$.

When $s_M = 0.75$ or 1 while σ_M is varied, the flutter boundaries obtained are shown, respectively, in Figs. 9(b) and (c). It can be seen in Fig. 9(b) that, when $s_M = 0.75$, the value of U_{Rc} increases monotonically

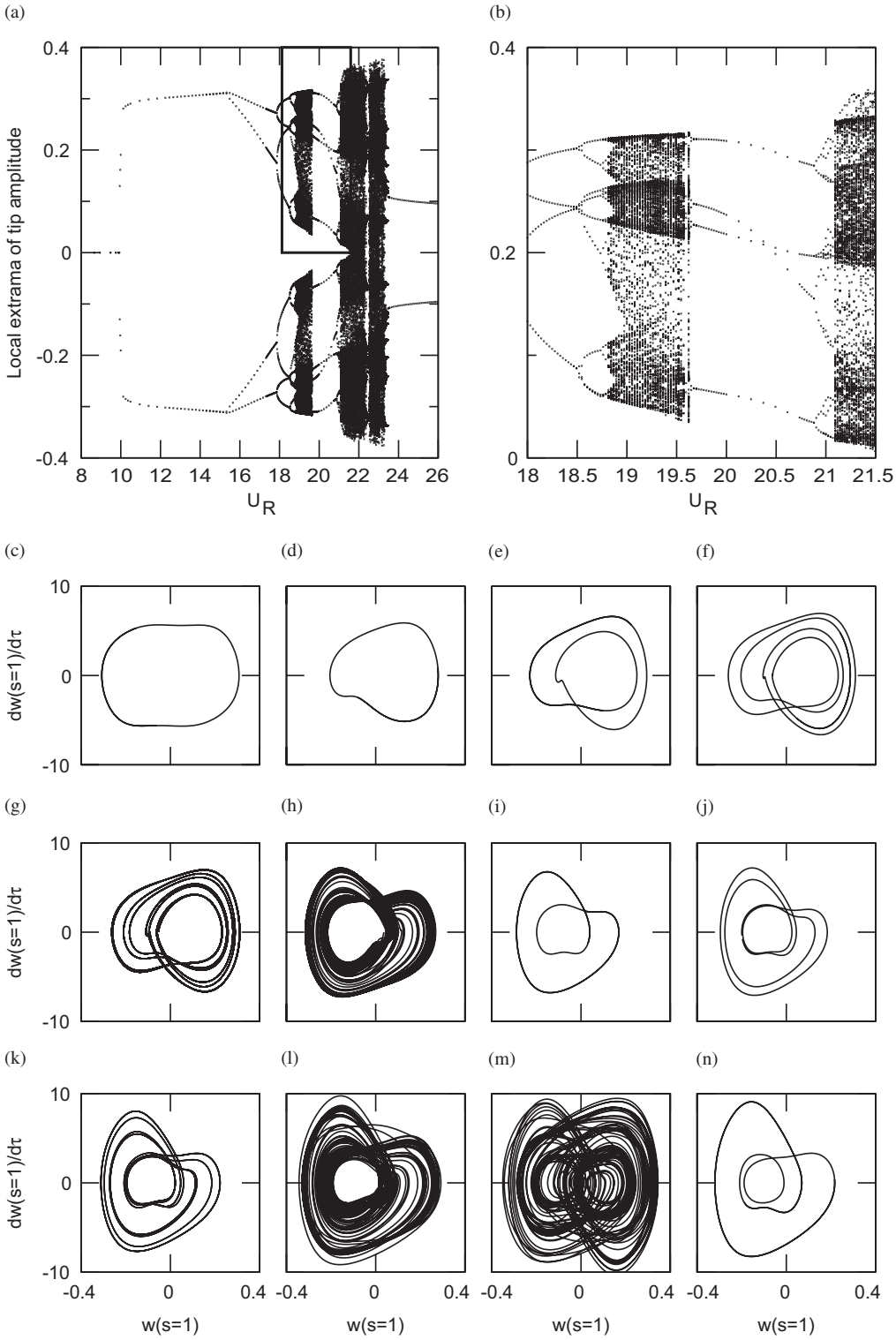

Fig. 7. The dynamics of a cantilevered flexible plate in axial flow with an additional cubic spring support at $s_S = 0.8$. (a) Bifurcation diagram; (b) enlargement of the block in (a); and, (c–n) the phase-plane plots at various values of U_R: (c) 14.14, (d) 17.32, (e) 18.17, (f) 18.71, (g) 18.79, (h) 19.49, (i) 20.74, (j) 20.95, (k) 21.02, (l) 21.21, (m) 21.91, and (n) 22.47. The system parameters are $\mu = 0.2$, $l_0 = 0.01$, $\alpha = 0.004$ and $C_D = 0$. The spring force is given by $f_S = -k_C w^3(s = 0.8)$, where $k_C = 6000$.

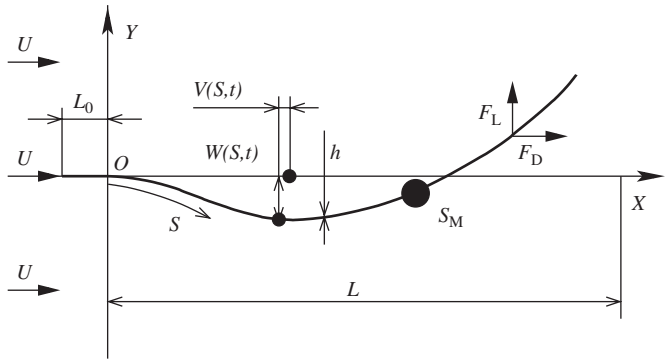

Fig. 8. A cantilevered flexible plate in axial flow with an additional concentrated mass.

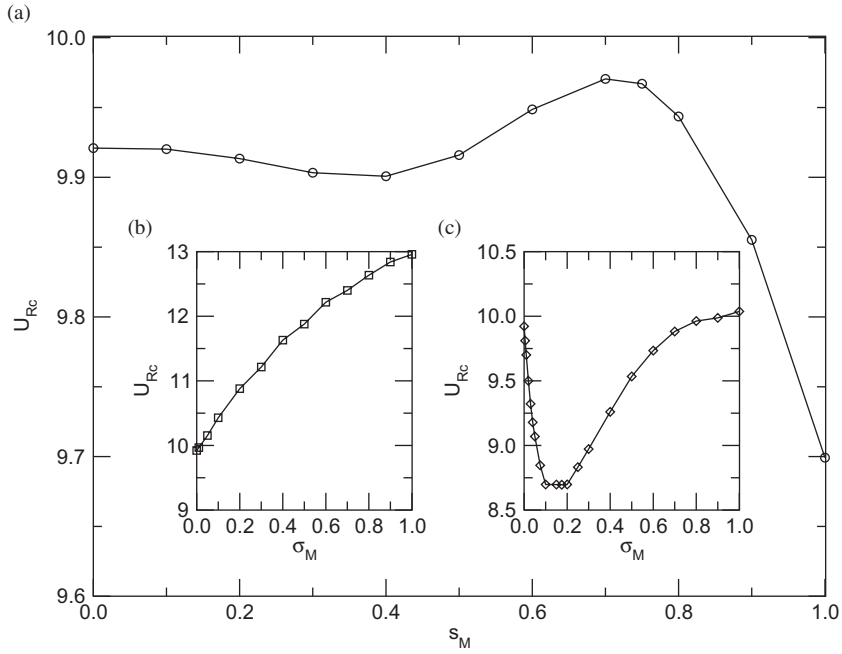

Fig. 9. The influence of an additional concentrated mass on stability: (a) $\sigma_M = 0.01$ while s_M is varied, (b) $s_M = 0.75$ while σ_M is varied, and (c) $s_M = 1$ while σ_M is varied. The other parameters of this system are $\mu = 0.2$, $l_0 = 0.01$, $\alpha = 0.004$ and $C_D = 0$.

from $U_{Rc} = 9.92$ for $\sigma_M = 0$ to $U_{Rc} = 12.96$ for $\sigma_M = 1$. When $s_M = 1$, the relation between U_{Rc} and σ_M becomes complicated: as shown in Fig. 9(c), U_{Rc} decreases significantly with increasing σ_M for $0 < \sigma_M < 0.1$; however, for $0.1 < \sigma_M < 0.2$, the variation in U_{Rc} is negligibly small, and a plateau is formed where $U_{Rc} = 8.70$. As σ_M is increased further, the trend for U_{Rc} is reversed; and, finally $U_{Rc} = 10.04$ when $\sigma_M = 1$. The pattern of the flutter boundary presented in Fig. 9(c) may be correlated to the vibration modes of the plate along the flutter boundary, as shown in Fig. 10. It is seen that, when σ_M is small, say $\sigma_M < 0.2$, the mode shapes of the plate in Figs. 10(a)–(e) are qualitatively the same; they are combinations of the first and second beam-mode shapes. In contrast, when $\sigma_M \geqslant 0.3$, as shown in Figs. 10(f)–(h), the vibration modes are mostly of second-beam-mode shape, and a quasi-stationary node becomes more prominent.

It has been observed in Fig. 9(a) that a small additional concentrated mass $\sigma_M = 0.01$ located at $s_M = 1$ significantly reduces the value of critical point; moreover, as shown in Fig. 11, it also affects the manner of the onset of the flutter and the post-critical dynamics of the system. It is seen in Fig. 11(a) that, as compared to the post-critical behaviour of the basic configuration, flutter takes place in a more abrupt manner; and, beyond

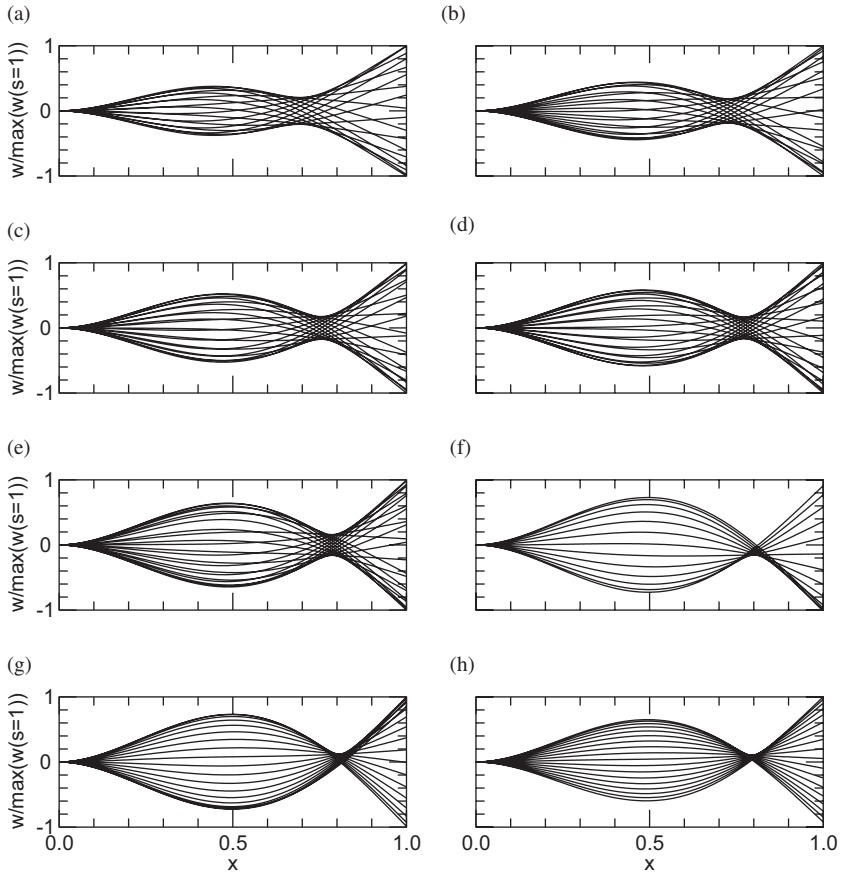

Fig. 10. The flutter modes of the system with an additional concentrated mass σ_M located at the trailing edge of the plate (i.e., $s_M = 1$): (a) $\sigma_M = 0.01$, (b) 0.05, (c) 0.1, (d) 0.15, (e) 0.2, (f) 0.3, (g) 0.6, and (h) 1. Note that these mode shapes are obtained at the critical point of each individual case. The other parameters of the system are $\mu = 0.2$, $l_0 = 0.01$, $\alpha = 0.004$ and $C_D = 0$.

the critical point, the flutter amplitude is rather large. This phenomenon may imply the occurrence of a subcritical bifurcation instead of a supercritical one.

With a small concentrated mass $\sigma_M = 0.01$ located at $s_M = 1$, symmetric limit cycle oscillations can still be observed at higher U_R beyond the critical point $U_{Rc} = 9.70$, as shown in Figs. 11(b), (d) and (g) for the case $U_R = 10.37$ for example. Note that the flutter amplitude of the system with an additional concentrated mass is significantly larger than that without, even though $\sigma_M = 0.01$ is so small. As U_R increases further and exceeds $U_R = 10.43$, chaos takes place, as shown in Figs. 11(e) and (h) for $U_R = 10.49$ where chaotic motions start to emerge, and in Figs. 11(f) and (i) for $U_R = 10.95$ where the dynamics of the system is fully chaotic.

A conventional route to chaos cannot be identified from the bifurcation diagram of Fig. 11(a). Closer examination of the dynamics regarding the onset of chaotic motions reveals that the rear part of the plate may whip forward, as illustrated by the two deformed shapes of the plate shown in thicker lines in Fig. 11(c) for the vibration modes of the system at $U_R = 10.49$; corresponding spikes in the phase-plane plot can be observed in the blocked region in Fig. 11(h). The spikes in the phase-plane plot can be more clearly observed in the two blocked regions in Fig. 11(i) for $U_R = 10.95$; the occurrence of one of these spikes is carefully studied in Fig. 12, where the time history, a section of the phase-plane plot and the vibration modes of the system are presented. It can be seen in Fig. 12(b) that a spike occurs at the point of the intersection of segments (1) and (2) in the section of the phase-plane plot. Note that, segments (1)–(3) can also be identified in Figs. 12(a) and (c)–(e); no spike-like phenomena are observed. That is, the spikes are likely not caused by numerical errors, as no corresponding jump or discontinuity is found in the time history and the vibration modes. Instead, as one can see from Figs. 12(c) and (d), the spike is caused by a jerk in the motion when the trailing edge of the plate

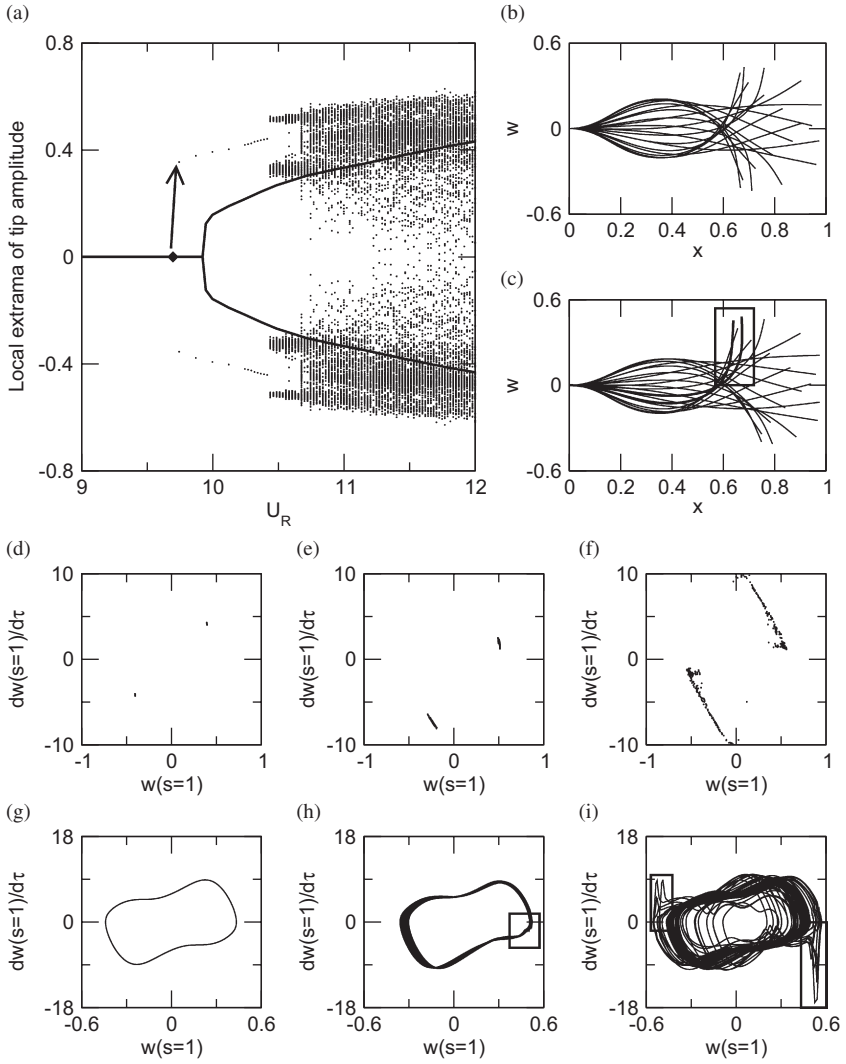

Fig. 11. The dynamics of the system with a small concentrated mass located at the trailing edge of the plate, i.e., $\sigma_M = 0.01$ and $s_M = 1$. (a) Bifurcation diagram; (b) vibration modes at $U_R = 10.37$; (c) vibration modes at $U_R = 19.49$; (d–f) Poincaré maps at various values of U_R: (d) $U_R = 10.37$, (e) 10.49, and (f) 10.95; and, (g–i) phase-plane plots at various values of U_R: (g) $U_R = 10.37$, (h) 10.49, and (i) 10.95. The other parameters of the system are $\mu = 0.2$, $l_0 = 0.01$, $\alpha = 0.004$ and $C_D = 0$. Note that the Poincaré maps are obtained by simultaneously recording the position and the velocity of the trailing edge of the plate with $w(s = 0.5) = 0$ as the controlling event. In subfigure (a): dot, the case $s_M = 1$ and $\sigma_M = 0.01$; solid line, the case without end-mass (i.e., the basic system).

is close to its local maximum amplitude (in the positive sense for the specific spike studied in Fig. 12): the small variations in the vibration modes are accompanied by large changes in the vibration velocity. Finally, it should be mentioned that the wrapped-around mode shapes predicted by the present theory may not be physically correct in terms of modelling of the fluid flow: there is concern in this case as to what extent the lumped vortex model [11] can be used to calculate the aero/hydro-dynamics at such large deflections of the plate. Nevertheless, the analysis herein provides a very interesting case of chaotic motions in conjunction with complex evolution of the mode shapes of the system.

6. With a small oscillating incidence angle

It is of interest to study the dynamics of the system when the undisturbed flow itself has an unsteady component, specifically a small oscillating component. For example, as shown in Fig. 13, the undisturbed flow

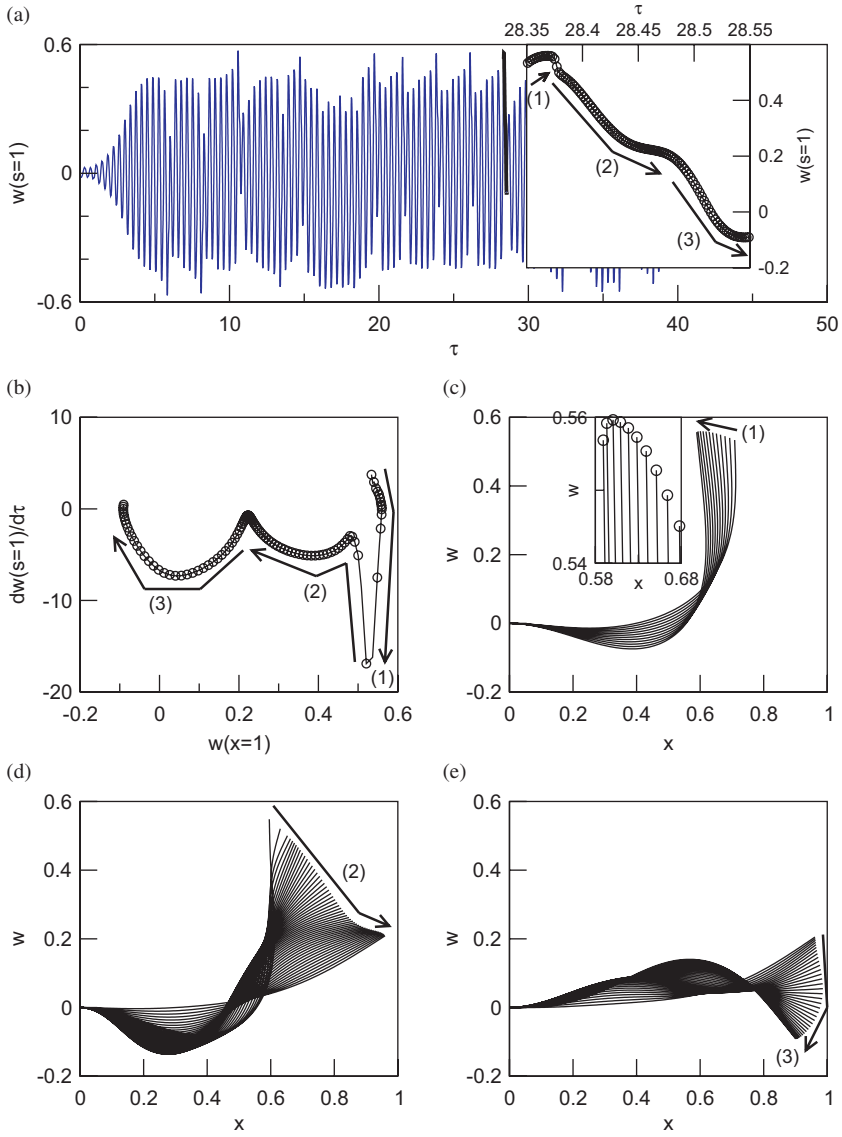

Fig. 12. The occurrence of the spurs observed in Fig. 11. (a) Time history; (b) phase-plane plot; and, (c–e) vibration modes. The parameters of the system are $\sigma_M = 0.01$, $s_M = 1$, $\mu = 0.2$, $U_R = 10.95$, $l_0 = 0.01$, $\alpha = 0.004$ and $C_D = 0$.

is considered to be not exactly parallel to the neutral plane of the plate (as compared to Fig. 1) although its speed is still U; it is supposed that the mean incident flow oscillates harmonically, with amplitude α_U and frequency f_{α_U}.

With a small oscillating incidence angle, the undistributed flow velocity can be decomposed into two parts in the fixed X–Y coordinate system as shown in Fig. 13, i.e.,

$$u_x = \cos[\alpha_U \cos(2\pi f^{\star}_{\alpha_U}\tau)], \quad u_y = \sin[\alpha_U \cos(2\pi f^{\star}_{\alpha_U}\tau)], \tag{14}$$

where u_x and u_y are, respectively, the flow velocity components in the x and y directions, normalized by U; $f^{\star}_{\alpha_U}$ is the nondimensional counterpart of f_{α_U} (refer to Eq. (4)). It follows that, when calculating the fluid loads, the aero/hydo-dynamics model of the system [11] should accordingly be modified to take into account both u_x and u_y. Moreover, it should be emphasized that a simplified model of the vortical wake behind the cantilevered flexible plate is adopted, as discussed in Ref. [11]. In the present investigation, it is assumed for simplicity that

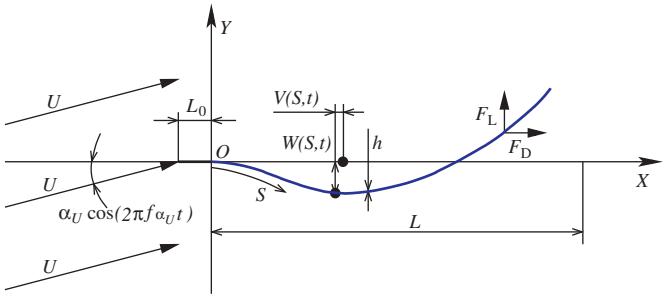

Fig. 13. A cantilevered flexible plate in axial flow with a small oscillating incidence angle.

the magnitude of the incidence angle α_U is so small that each individual wake vortex, once it is shed off the trailing edge of the plate, still moves downstream with the velocity of the undisturbed flow as if the angle of incidence were always $\alpha_U \equiv 0$.

The dynamics of the system with $f^{\star}_{\alpha_U} = 0$ is examined first, i.e., a fixed small angle of incidence. (It should be mentioned that this may find application in the design of the flexible control surface attached to a rigid wing [9], where the cantilevered flexible plate is not always parallel to the undisturbed flow.) It can be seen in Fig. 14(a) that, as compared to the system in the basic configuration (i.e., $\alpha_U = 0$), the plate is subjected to a static deformation before flutter takes place at sufficiently high U_R. For a small incidence angle ($\alpha_U = 5^{\circ}$), $U_{Rc} = 9.87$ is obtained, which is slightly below the critical point $U_{R_c^{\star}} = 9.92$ for the system set up in the basic configuration. As shown in Fig. 14(b), before the onset of flutter, the amplitude of the static deformation grows as U_R increases; and the plate deforms in the first beam mode. But, when $U_R > U_{Rc}$, the vibration modes of the system, shown in Figs. 14(c) and (d), are found to be qualitatively the same as those of the system in the basic configuration (see Ref. [11]). However, the vibration of the plate is not symmetric with respect to its neutral plane; instead, the static component can be observed in the vibration modes.

When $f^{\star}_{\alpha_U} \neq 0$, rich dynamics of the system is obtained. The influence of $f^{\star}_{\alpha_U}$ is studied in Fig. 15, in which the magnitude of the incidence angle is $\alpha_U = 5^{\circ}$ and the frequency is swept from $f^{\star}_{\alpha_U} = 0$ to 20. Note that the reduced flow velocity U_R used in the frequency sweep is $U_R = 8.94$, which is about 10% below the critical point of either the case of a fixed incidence angle with $\alpha_U = 5^{\circ}$ (as seen in Fig. 14(a), $U_{Rc} = 9.87$) or the case of the system in the basic configuration (i.e., for $\alpha_U = 0^{\circ}$ and $f^{\star}_{\alpha_U} = 0$, for which $U_{Rc} = 9.92$).

In Fig. 15(a), resonance phenomena in the frequency–response of the system can be observed. If the vibration amplitude of the plate is evaluated at the tailing edge, i.e., the point $s = 1$, three local peaks can be found: at $f^{\star}_{\alpha_U} = 1.15$, 2.8 and 9.4. However, when observed at the plate mid-length point $s = 0.5$, the first two peaks shift to $f^{\star}_{\alpha_U} = 0.95$, 2.81, respectively; moreover, the third peak disappears. It is evident that the primary resonance of the system occurs at $f^{\star}_{\alpha_U} = 2.8$ (or $f^{\star}_{\alpha_U} = 2.81$ in terms of the amplitude at $s = 0.5$), where the plate vibrates with quite a large amplitude. The pattern of the frequency–response shows that an external excitation [15], i.e., the small oscillating incidence angle, has been applied to the system. However, it should be noted that, although the oscillation of the incidence angle is an external excitation, the undisturbed flow and the plate are two inseparable parts of an integrated system; the aero/hydro-dynamic forces caused by the fluid flow (with a small oscillating angle of incidence) depend on the motions of the plate. Therefore, it does not make sense to talk about the natural frequency of the plate without taking into account the fluid flow. Under these circumstances, one cannot expect the secondary resonances of the system to be related to the primary one *via* an integer relationship (either subharmonic or superharmonic). In particular, in the current case, the secondary resonances of the system can be found at $f^{\star}_{\alpha_U} = 1.15$ and 9.4 in terms of the amplitude at $s = 1$, and the ratios to the primary resonance of $f^{\star}_{\alpha_U} = 2.8$ are, respectively, 0.4107 and 3.357.

The dynamics of system for the case $f^{\star}_{\alpha_U} = 2.8$ is shown in Figs. 15(b)–(e); one can see that the vibration of the plate, at the primary resonance point, is very similar to that of the system in the basic configuration [11]. Additionally, it is found that the system vibrates with only one frequency which is exactly the same as the excitation frequency, i.e., $f^{\star}_{\alpha_U}$.

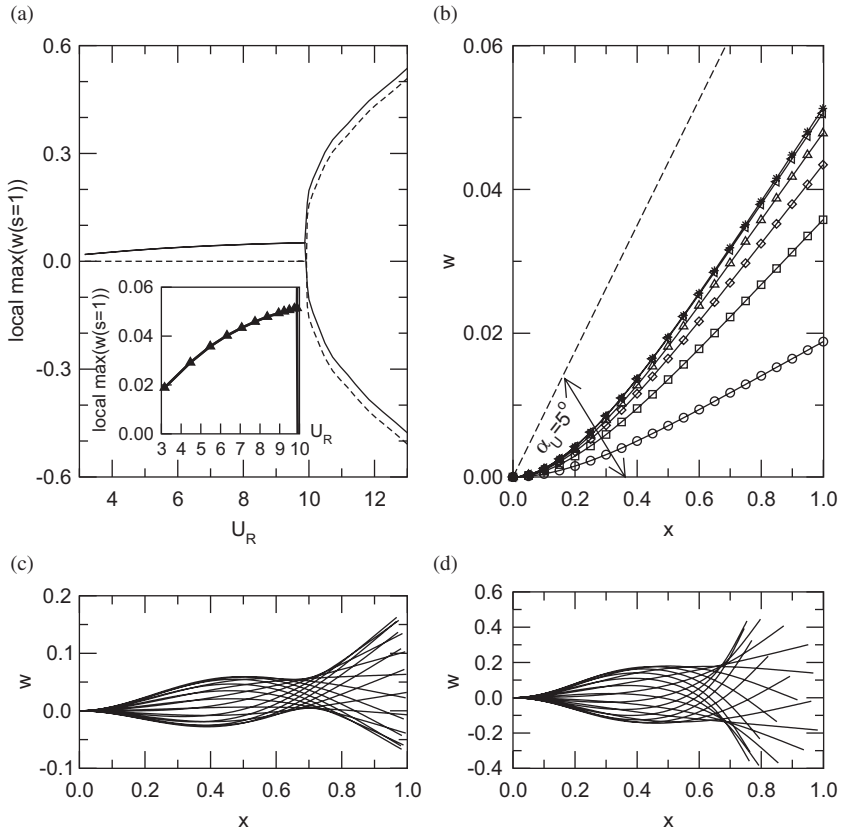

Fig. 14. The dynamics of a cantilevered flexible plate in axial flow with a fixed small incidence angle: $\alpha_U = 5^o$ and $f^{\star}_{\alpha_U} = 0$: (a) bifurcation diagram, (b) buckled states when $U_R < U_{Rc}$, (c) vibration modes of small amplitude flutter at $U_R = 9.95$, and (d) vibration modes of large amplitude flutter at $U_R = 11.83$. The other parameters of the system are $\mu = 0.2$, $l_0 = 0.01$, $\alpha = 0.004$ and $C_D = 0$. In subfigure (a): solid line, the case $\alpha_U = 5^o$ and $f^{\star}_{\alpha_U} = 0$; dashed-line, $\alpha_U = 0^o$ (i.e., the basic system). In subfigure (b): the lines with various symbols: circle, $U_R = 3.16$; square, $U_R = 5.48$; diamond, $U_R = 7.07$; up-triangle, $U_R = 8.37$; left-triangle, $U_R = 9.49$; star, $U_R = 9.75$.

The vibration modes of the system at various values of $f^{\star}_{\alpha_U}$ are shown in Fig. 16, normalized by the maximum amplitude in each case (not necessarily at $s = 1$ or 0.5). It is interesting to see that the vibration modes of the plate depend on $f^{\star}_{\alpha_U}$. When $f^{\star}_{\alpha_U}$ is small, the plate vibrates in the first beam mode; however, beam modes of higher order participate in the vibration and become increasingly important in the dynamics as $f^{\star}_{\alpha_U}$ increases. Moreover, when the first and second beam modes are dominant in the dynamics of the system, the maximum amplitude of the plate takes place at $s = 1$; while, when beam modes of higher order become important, the maximum amplitude occurs near the middle of the plate.

When examining the frequency–response in conjunction with the vibration modes of the system, as in Figs. 15(a) and 16, more important observations with regard to the dynamics of the system can be made. First, since the vibration mode of the system changes with varying $f^{\star}_{\alpha_U}$, the resonance points of the system depend on the point of observation. For example, the secondary resonance occurs at $f^{\star}_{\alpha_U} = 1.15$ if it observed at the point $s = 1$, while it is located at $f^{\star}_{\alpha_U} = 0.95$ if the point $s = 0.5$ is chosen for observing the frequency–response of the system. Second, at the primary resonance point $f^{\star}_{\alpha_U} = 2.8$ (or $f^{\star}_{\alpha_U} = 2.81$ in terms of the vibration amplitude at $s = 0.5$), the plate vibrates in the second beam mode, and the frequency–response curve slightly bends to the left, which implies a weak softening-type nonlinearity in the fluid–structure interaction system [15]. In contrast, at the secondary resonance point $f^{\star}_{\alpha_U} = 1.15$ (or $f^{\star}_{\alpha_U} = 0.95$ in terms of the vibration amplitude at $s = 0.5$), the frequency–response curve slightly bends to the right; therefore, a hardening-type nonlinearity arises when the plate vibrates in the first beam mode at low $f^{\star}_{\alpha_U}$. It should be mentioned that investigations on the properties of the nonlinearity in a two-dimensional cantilevered flexible plate (modelled using the

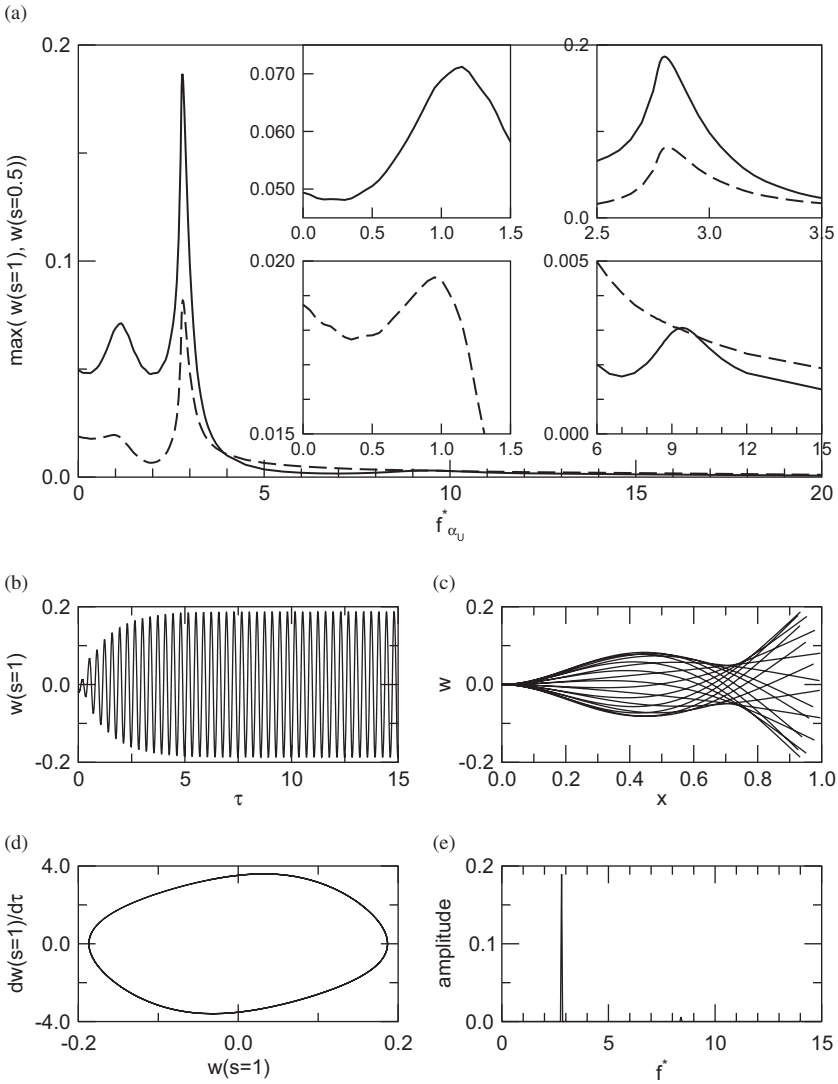

Fig. 15. The frequency–response of a cantilevered flexible plate in axial flow with a small oscillating incidence angle, where $\alpha_U = 5^o$ and the value of $f^{\star}_{\alpha_U}$ is swept from 0 to 20. (a) Frequency–response of the system; (b–e) the dynamics of the system when $f^{\star}_{\alpha_U} = 2.8$: (b) time history, (c) vibration modes, (d) phase-plane plot, and (e) vibration frequency. The other parameters of the system are $\mu = 0.2$, $U_R = 8.94$, $l_0 = 0.01$, $\alpha = 0.004$ and $C_D = 0$. In subfigure (a): solid line, $w(s = 1)$; dashed-line, $w(s = 0.5)$.

inextensibility assumption), instead of the whole fluid–structure interaction system, were previously conducted by Anderson et al. [16] and Tang et al. [14], and similar conclusions have been reached. Finally, when $f^{\star}_{\alpha_U}$ is close to zero, the plate vibrates in the first beam mode with an amplitude smaller than that of the static buckling state obtained using $f^{\star}_{\alpha_U} = 0$.

7. Concluding remarks

In the present paper, the dynamics of four variants of two-dimensional cantilevered flexible plates in axial flow are studied: with (i) a gravitational force, (ii) a spring support, (iii) a concentrated mass, and (iv) an oscillating incidence angle in the undisturbed flow. Additional parameters arise in the model of the system when a new feature is taken into account; their influence on the dynamics of the system, in terms of the magnitude and/or location in the case of (ii) and (iii), are investigated. It has been shown that the new features

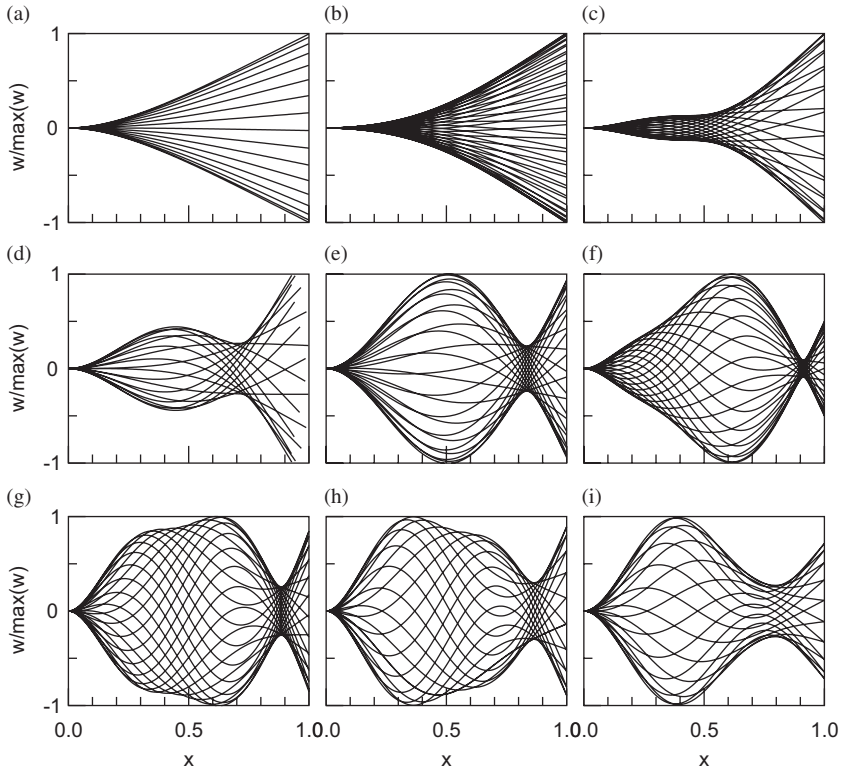

Fig. 16. The vibration modes of a cantilevered flexible plate in axial flow with a small oscillating incidence angle, where $\alpha_U = 5^{\circ}$ and $f^{\star}_{\alpha_U}$ is varied: (a) $f^{\star}_{\alpha_U} = 0.3$, (b) 1.15, (c) 2, (d) 2.8, (e) 4, (f) 8, (g) 9, (h) 9.5 and (i) 11. The other parameters of the system are $\mu = 0.2$, $U_R = 8.94$, $l_0 = 0.01$, $\alpha = 0.004$ and $C_D = 0$.

added to the system may qualitatively alter the dynamics, both in terms of the critical point and the post-critical behaviour. Some interesting findings, for example, buckled states, chaotic motions, stronger-constraint/less-stable-system phenomenon, jerk-like motions, and complicated patterns of frequency–response are summarized in this paper.

Acknowledgement

The leading author is supported by the Open Research Fund Program of Hubei Provincial Key Laboratory of Fluid Machinery and Power Engineering Equipment, and a Natural Sciences and Engineering Research Council of Canada (NSERC) Post-Doctoral Fellowship. The support of NSERC for this research is also gratefully acknowledged.

References

[1] M.P. Païdoussis, *Fluid–Structure Interactions. Slender Structures and Axial Flow*, Vol. 2, Elsevier Academic Press, London, 2004.
[2] A. Kornecki, E.H. Dowell, J. O'Brien, On the aeroelastic instability of two-dimensional panels in uniform incompressible flow, *Journal of Sound and Vibration* 47 (1976) 163–178.
[3] A. Kornecki, Aeroelastic and hydroelastic instabilities of infinitely long plates. I, *SM Archives* 3 (1978) 381–440.
[4] E.H. Dowell, *Aeroelasticity of Plates and Shells*, Noordhoff International Publishing, Leyden, 1975.
[5] Y.B. Chang, P.M. Moretti, Flow-induced vibration of free edges of thin films, *Journal of Fluids and Structures* 16 (2002) 989–1008.
[6] Y. Watanabe, S. Suzuki, M. Sugihara, Y. Sueoka, An experimental study of paper flutter, *Journal of Fluids and Structures* 16 (2002) 529–542.
[7] Y. Watanabe, K. Isogai, S. Suzuki, M. Sugihara, A theoretical study of paper flutter, *Journal of Fluids and Structures* 16 (2002) 543–560.

[8] J.J. Allen, A.J. Smits, Energy harvesting eel, *Journal of Fluids and Structures* 15 (2001) 629–640.
[9] R. de Breuker, M.M. Abdalla, Z. Gürdal, Flutter of partially rigid cantilevered two-dimensional plates in axial flow, *AIAA Journal* 46 (2008) 936–946.
[10] M.S. Triantafyllou, A.H. Techet, F.S. Hover, Review of experimental work in biomimetic foils, *IEEE Journal of Oceanic Engineering* 29 (2004) 585–594.
[11] L. Tang, M.P. Païdoussis, On the instability and the post-critical behavior of two-dimensional cantilevered flexible plates in axial flow, *Journal of Sound and Vibration* 305 (2007) 97–115.
[12] L. Tang, M.P. Païdoussis, J. Jiang, Cantilevered flexible plates in axial flow: energy transfer and the concept of flutter-mill, *Journal of Sound and Vibration*, submitted for publication.
[13] J. Zhang, S. Childress, A. Libchaber, M. Shelley, Flexible filaments in a flowing soap film as a model for one-dimensional flags in a two-dimensional wind, *Nature* 408 (2000) 835–839.
[14] D.M. Tang, H. Yamamoto, E.H. Dowell, Flutter and limit cycle oscillations of two-dimensional panels in three-dimensional axial flow, *Journal of Fluids and Structures* 17 (2003) 225–242.
[15] J.J. Thomsen, *Vibrations and Stability, Order and Chaos*, McGraw-Hill, London, 1997.
[16] T.J. Anderson, A.H. Nayfeh, B. Balachandran, Experimental verification of the importance of the nonlinear curvature in the response of a cantilevered beam, *Journal of Vibration and Acoustics* 118 (1996) 21–27.